11th World Congress on Computational Mechanics (WCCM XI)
5th European Conference on Computational Mechanics (ECCM V)
6th European Conference on Computational Fluid Dynamics (ECFD VI)
E. Oñate, J. Oliver and A. Huerta (Eds)

BRIDGING MULTI-SCALE METHOD TO CONSIDER THE EFFECTS OF LOCAL DEFORMATIONS IN THE ANALYSIS OF COMPOSITE THIN-WALLED MEMBERS

R. EMRE ERKMEN[†], ASHKAN AFNANI[*]

[†] Centre for Built Infrastructure Research, Faculty of Engineering and IT, University of Technology, Sydney, P.O. Box 123 Broadway, NSW, Australia emre.erkmen@uts.edu.au

[*] Centre for Built Infrastructure Research, Faculty of Engineering and IT, University of Technology, Sydney, P.O. Box 123 Broadway, NSW, Australia ashkan.afnaniEsfandabadi@student.uts.edu.au

Key Words: *Multi-scale, Composite, Thin-walled, local buckling, Decomposition method*

Abstract. Thin-walled member composed of fibre-reinforced polymer composite laminates that have one dimension relatively large in comparison to their cross-sectional dimensions are conventionally modelled by one dimensional beam-type finite elements. Due to the rigid cross section assumption in the formulation of this class of elements, only beam-axis-related deformations can be considered, including flexural, torsional and lateral buckling. However, local deformations such as local buckling of web and flanges, which might have significant effects on the global response of the member, are ignored. In order to model these types of deformations, shell-type elements are used throughout the domain of the member. While the former lacks accuracy in some cases, the latter creates oversized models that are computationally uneconomical. The purpose of the current study is to develop a finite element model to consider the local effects by a multi-scale overlapping decomposition method. In this method, beam-type elements are used as a basis for the whole domain of the member while shell-type elements are placed in critical regions only to incorporate the local effect on the global behaviour. Therefore, it allows considering the local deformations in the numerical analysis without using shell-type elements throughout the domain. Numerical examples are provided in which the results are compared to the full-shell-type model, indicating the efficiency and accuracy of the proposed technique.

1 INTRODUCTION

The use of fibre-reinforced polymer composite laminated plates as a construction material has increased in recent years. The main reasons of this increase are favourable properties that these types of material possess, namely, non-corrosive nature and prolonged durability, high tensile strength-to-weight ratio, electromagnetic neutrality and resistance to chemical attack. Their high strength-to-weight ratio allows fabrication of slender structural components, the spans of which are often large in comparison to their cross-sectional dimension. Therefore, beam-type finite elements are normally used for their analysis. A beam formulation was developed by Bauld & Tzeng [1] to capture flexural and lateral-torsional buckling behaviour

of thin-walled composite laminated members. Closed form analytical solutions for buckling analysis based on the beam-type formulation have been developed (e.g. [2-5]), the use of which is limited to simple loading and boundary conditions. On the other hand, finite element formulations [6-10] can be used to obtain flexural-torsional buckling behaviour of composite thin-walled members with general loading and boundary conditions. However, these types of elements are formulated by rigid cross-section assumption and consequently are not able to consider cross-sectional deformations such as the local buckling in web or flange and distortional buckling. Alternatively, should the cross-sectional deformations be of interest, one has to perform a more complicated shell-type analysis for the whole domain of the structure.

Recent focus of research on computational mechanics has been on adaptive numerical methods such as mechfree methods (e.g. [11, 12]), Generalized finite element method (e.g. [13,14]) and Multi-scale methods [15-20], which allow the implementation of more accurate numerical models only at the regions of interest (i.e. where local deformations exist) while keeping the rest of the domain to be modelled by the simpler models. Particularly, the Bridging Multiscale Method (BMM), which was originally developed to enrich the nodal values of the FEM solution with meshfree solutions [21], provides a basis to couple problems based on two different physical assumptions (e.g. [22]). BMM allows the separation of the local analysis, which is based on comparatively sophisticated modelling assumptions, from the global analysis, in which rather simplistic assumptions are implemented.

Thin-walled beam behaviour also give rise to multiple scales in the deformations with multiple scales due to the interaction of the local buckling (i.e. cross-sectional/local deformations) and the global buckling modes [23]. In order to capture local buckling behaviour, several methodologies have been utilized; namely finite strip formulations (e.g. [24]), the generalized beam theory (e.g. [25]), and shell-type elements (e.g. [26]). Recently, Erkmen [27] developed a numerical technique based on BMM to consider the effect of the local deformations on the global behaviour of the thin-walled structure. This method allows the use of different kinematic assumptions in the local and global model. Therefore, simple beam-type numerical models were used to evaluate the global behaviour, and more detailed shell-type models were used in the place of localized behaviour. In the present study, the application of the method is expanded for composite thin-walled members. In order to specify the efficiency and accuracy of the method, the results are compared to the beam and full shell-type models.

2 BEAM-TYPE ANALYSIS

The beam-type analysis, which is used for the analysis of the whole domain, is based on classical thin-walled beam theory. The kinematic assumptions of the theory lead to a strain vector consisting of axial strain due to the bending, membrane and torsional actions, and shear strains resulting from torsion only. The strain components can be written in terms of displacements parallel to $\bar{x}$, $\bar{y}$ and $\bar{z}$ directions, i.e. $\bar{u}(\bar{z}), \bar{v}(\bar{z})$ and $\bar{w}(\bar{z})$, respectively, the angle of twist of the cross-section $\bar{\phi}$ and their derivatives. The strain vector is decomposed into linear and nonlinear components, i.e. $\bar{\boldsymbol{\varepsilon}} = \bar{\boldsymbol{\varepsilon}}_L + \bar{\boldsymbol{\varepsilon}}_N$. Each part can be obtained by multiplying the matrix of cross-sectional coordinates $\bar{\mathbf{S}}$ by linear and nonlinear vectors

including displacement components.

$$\bar{\boldsymbol{\varepsilon}}_L = \langle \bar{\varepsilon}_L \quad 0 \quad \bar{\gamma}_L \quad 0 \rangle^{\mathrm{T}} = \bar{\mathbf{S}}\bar{\boldsymbol{\chi}}_L$$
$$\bar{\boldsymbol{\varepsilon}}_N = \langle \bar{\varepsilon}_N \quad 0 \quad \bar{\gamma}_N \quad 0 \rangle^{\mathrm{T}} = \mathbf{S}\bar{\boldsymbol{\chi}}_N \tag{1}$$

Where

$$\bar{\mathbf{S}} = \begin{bmatrix} 1 & -\bar{x} & -\bar{y} & -\bar{\omega} & \bar{x}^2+\bar{y}^2 & 0 \\ 0 & 0 & 0 & 0 & 0 & 0 \\ 0 & 0 & 0 & 0 & 0 & -2\bar{r} \\ 0 & 0 & 0 & 0 & 0 & 0 \end{bmatrix} \tag{2}$$

And

$$\bar{\boldsymbol{\chi}}_L{}^{\mathrm{T}} = \langle \bar{w}' \quad \bar{u}'' \quad \bar{v}'' \quad \bar{\phi}'' \quad 0 \quad \bar{\phi}' \rangle \tag{3}$$

while the nonlinear displacement vector can be considered as follows, based on Trahair [28]

$$\bar{\boldsymbol{\chi}}_N{}^{\mathrm{T}} = \left\langle \frac{1}{2}\left(\bar{u}'^2+\bar{v}'^2\right) - a_x\bar{v}'\bar{\phi}' + a_y\bar{u}'\bar{\phi}' + \frac{1}{2}\left(a_x{}^2+a_y{}^2\right)\bar{\phi}'^2 \quad \bar{v}''\bar{\phi} + a_x\bar{\phi}'^2 \quad -\bar{u}''\bar{\phi} + a_y\bar{\phi}'^2 \quad 0 \quad \frac{1}{2}\bar{\phi}'^2 \quad 0 \right\rangle \tag{4}$$

In Eq. (2), $\bar{x}$ and $\bar{y}$ denote the coordinates of a point on the cross-section, $\bar{r}$ is the normal distance from the mid-surface and the sectorial coordinate $\bar{\omega} = \int h d\bar{s}$ has been used, in which h is the normal distance to the tangent of the point on the section contour from the arbitrarily located pole with $\bar{x}$ and $\bar{y}$ coordinates (a_x, a_y).

A finite element is formulated by assuming linear interpolation for $\bar{w}$ and cubic interpolations for $\bar{u}$, $\bar{v}$ and $\bar{\phi}$. Based on the above mentioned assumptions, the variational formulation can be formed to obtain the equilibrium equation as

$$\delta\bar{\Pi} = \int_L \int_A \delta\bar{\boldsymbol{\varepsilon}}^{\mathrm{T}}\bar{\boldsymbol{\sigma}}\mathrm{d}A\,\mathrm{d}\bar{z} - \delta\bar{\mathbf{d}}^{\mathbf{T}}\bar{\mathbf{f}} = 0 \tag{5}$$

In Eq. (5), A is the cross-sectional area; L is the length of the beam and $\bar{\mathbf{f}}$ is the external load vector. The stress expression can be obtained directly from the strains using the linear stress-strain relationship for an isotropic material. Consequently, the first variation of the strain vector can be written as

$$\delta\bar{\boldsymbol{\varepsilon}} = \bar{\mathbf{S}}\bar{\mathbf{B}}\delta\bar{\mathbf{d}} \tag{6}$$

The incremental equilibrium equations can be obtained by subtracting the virtual work expressions at two neighbouring equilibrium states and then linearizing the result by omitting the second- and higher-order terms, i.e.

$$\delta\left(\delta\bar{\Pi}\right) \approx \delta\bar{\mathbf{d}}^{\mathbf{T}}\bar{\mathbf{K}}\delta\bar{\mathbf{d}} - \delta\bar{\mathbf{d}}^{\mathbf{T}}\delta\bar{\mathbf{f}} = 0 \tag{7}$$

Where $\bar{\mathbf{K}}$ is the stiffness matrix of the global beam model, i.e.

$$\bar{\mathbf{K}} = \int_L \int_A \bar{\mathbf{B}}^{\mathrm{T}} \bar{\mathbf{S}}^{\mathrm{T}} \bar{\mathbf{E}} \bar{\mathbf{S}} \bar{\mathbf{B}} \mathrm{d}A \mathrm{d}\bar{z} + \int_L \bar{\mathbf{M}}_{\sigma} \mathrm{d}\bar{z} \tag{8}$$

in which $\bar{\mathbf{M}}_{\sigma} \delta \bar{\mathbf{d}} = \delta \bar{\mathbf{B}}^{\mathrm{T}} \int_A \bar{\mathbf{S}}^{\mathrm{T}} \bar{\boldsymbol{\sigma}} \mathrm{d}A$.

2.1 Constitutive relations for the beam element

It is assumed that perfect interlaminar bond exists between the layers. For a laminate composed of n orthotropic layers, the orientation of the local $\bar{s}_k \bar{z}_k$-plane with respect to the global $\bar{s}\bar{z}$-plane is determined by the angle about the $\bar{r}$-axis Φ between $\bar{z}$ and $\bar{z}_k$ (Figure 1(b)).

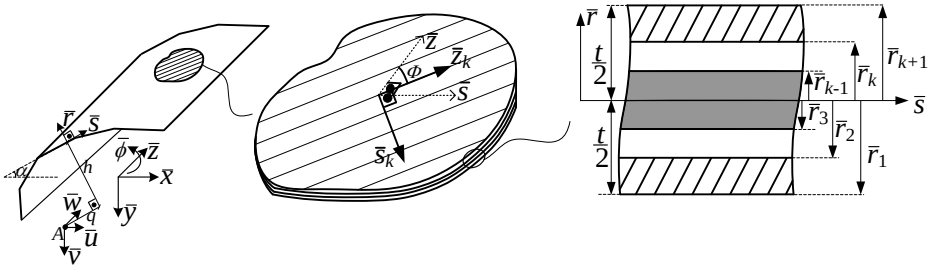

(a) Thin-walled beam (b) Fibre orientations (c) Laminates across the thickness

Figure 1: Thin-walled beam composed of fibre-reinforced laminates

For the k^{th} layer, the stress-strain relationship can be written as [9-11]

$$\bar{\boldsymbol{\sigma}}^{(k)} = \begin{Bmatrix} \bar{\sigma}_z{}^{(k)} \\ 0 \\ \bar{\tau}_{zs}{}^{(k)} \\ 0 \end{Bmatrix} = \bar{\boldsymbol{Q}}^{(k)} \bar{\boldsymbol{\varepsilon}} \tag{9}$$

where

$$\bar{\mathbf{Q}}^{(k)} = \begin{bmatrix} \bar{Q}_{11}{}^{*(k)} & 0 & \bar{Q}_{16}{}^{*(k)} & 0 \\ 0 & 0 & 0 & 0 \\ \bar{Q}_{16}{}^{*(k)} & 0 & \bar{Q}_{66}{}^{*(k)} & 0 \\ 0 & 0 & 0 & 0 \end{bmatrix} \tag{9}$$

in which $\bar{Q}_{11}{}^{*(k)} = \bar{Q}_{11}{}^{(k)} - \bar{Q}_{12}{}^{(k)2} / \bar{Q}_{22}{}^{(k)}$, $\bar{Q}_{16}{}^{*(k)} = \bar{Q}_{16}{}^{(k)} - \bar{Q}_{12}{}^{(k)} \bar{Q}_{26}{}^{(k)} / \bar{Q}_{22}{}^{(k)}$ and $\bar{Q}_{66}{}^{*(k)} = \bar{Q}_{66}{}^{(k)} - \bar{Q}_{26}{}^{(k)2} / \bar{Q}_{22}{}^{(k)}$ [9,11]. These coefficients can be found in [7-9, 29].

3 SHELL –TYPE ANALYSIS

In order to capture the buckling behaviour of the thin-walled member, a four-node shell element with 6 degrees of freedom per node is adopted. In order to satisfy C^1 continuity requirement of Kirchhoff plate theory and avoid shear locking effects, Discrete Kirchhoff Quadrilateral (Batoz & Tahar [30]) is chosen for the plate component, in which shear

deformations effects across the thickness is omitted. For the membrane component, the finite element of Ibrahimbegovic et al. [31] employing drilling degrees of freedom is adopted herein. Displacement degrees of freedom include bending rotations $\hat{\theta}_x$ and $\hat{\theta}_y$ in local xz and yz planes, drilling rotation $\hat{\theta}_x$ around z direction, deflections $\hat{u}_0$ and $\hat{v}_0$ of the mid-surface in local xy plane, and the out of plane deflection $\hat{w}_0$ in local z direction (Fig. 2.a)

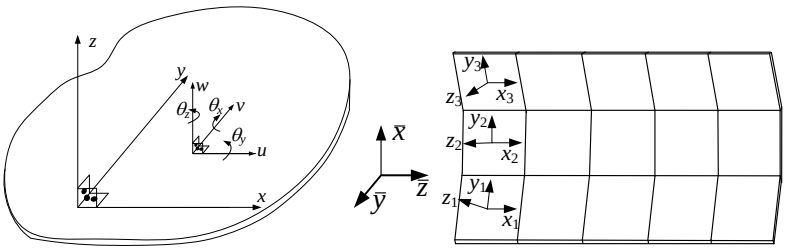

(a) Local deflections of the shell element (b) Global vs. local coordinate system

Figure 2: Deflections and coordinate systems of the shell formulations

The out of plane deflection $\hat{w}$ is interpolated linearly while the standard bilinear interpolation is used for the independent drilling rotation $\hat{\theta}_z$, and the Allman-type interpolation functions are used for the in-plane displacements $\hat{u}_0$ and $\hat{v}_0$ [31]. The equilibrium equations of the shell model is obtained in the variational form as

$$\delta\hat{\Pi} = \int_L \int_A \delta\hat{\boldsymbol{\varepsilon}}^{\mathrm{T}} \hat{\boldsymbol{\sigma}} \mathrm{d}A\mathrm{d}\bar{z} - \delta\hat{\mathbf{d}}^{\mathrm{T}} \hat{\mathbf{f}} = 0 \tag{10}$$

$\hat{\boldsymbol{\varepsilon}}$ in Eq. (10) represents the strain vector, which can be composed of strains due to plate bending $\hat{\boldsymbol{\varepsilon}}_b$, membrane action $\hat{\boldsymbol{\varepsilon}}_{mm}$, and strains due to second order membrane and plate bending action $\hat{\boldsymbol{\varepsilon}}_N$, i.e.

$$\hat{\boldsymbol{\varepsilon}} = \hat{\boldsymbol{\varepsilon}}_b + \hat{\boldsymbol{\varepsilon}}_{mm} + \hat{\boldsymbol{\varepsilon}}_N \tag{11}$$

where the plate bending strains can be written as

$$\hat{\boldsymbol{\varepsilon}}_b = -z \begin{Bmatrix} \dfrac{\partial \hat{\theta}_x}{\partial x} \\ \dfrac{\partial \hat{\theta}_y}{\partial y} \\ \dfrac{\partial \hat{\theta}_x}{\partial y} + \dfrac{\partial \hat{\theta}_y}{\partial x} \\ \hdashline 0 \end{Bmatrix} = -z \begin{Bmatrix} \hat{\boldsymbol{\chi}} \\ \hdashline 0 \end{Bmatrix} \tag{12}$$

in which $\hat{\boldsymbol{\chi}}$ is the curvature vector. The second term in Eq. (11) can be written as

$$\hat{\boldsymbol{\varepsilon}}_{mm} = \begin{Bmatrix} \dfrac{\partial \hat{u}_0}{\partial x} \\ \dfrac{\partial \hat{v}_0}{\partial y} \\ \dfrac{\partial \hat{u}_0}{\partial y} + \dfrac{\partial \hat{v}_0}{\partial x} \\ \hline \dfrac{1}{2}\left(\dfrac{\partial \hat{v}_0}{\partial x} - \dfrac{\partial \hat{u}_0}{\partial y} \right) - \hat{\theta}_z \end{Bmatrix} = \begin{Bmatrix} \hat{\boldsymbol{\varepsilon}}_m \\ \hline \dfrac{1}{2}\left(\dfrac{\partial \hat{v}_0}{\partial x} - \dfrac{\partial \hat{u}_0}{\partial y} \right) - \hat{\theta}_z \end{Bmatrix} \tag{13}$$

in which $\hat{\boldsymbol{\varepsilon}}_{mm}$ is the vector of membrane strains and the last row in Eq. (13) contains the skew symmetric part of the membrane strains introduced to avoid numerical stability issues when drilling rotations $\hat{\theta}_z$ are used with Allman-type interpolations. The non-linear strain component can be written as

$$\hat{\boldsymbol{\varepsilon}}_N = \begin{Bmatrix} \dfrac{1}{2}\left(\dfrac{\partial \hat{w}_0}{\partial x} \right)^2 + \dfrac{1}{2}\left(\dfrac{\partial \hat{v}_0}{\partial x} \right)^2 \\ \dfrac{1}{2}\left(\dfrac{\partial \hat{w}_0}{\partial y} \right)^2 \\ 0 \\ \hline 0 \end{Bmatrix} \tag{14}$$

Similar to the beam model, the equilibrium is obtained by the variational principle as

$$\delta \hat{\Pi} = \int_L \int_A \delta \hat{\boldsymbol{\varepsilon}}^{\mathrm{T}} \hat{\boldsymbol{\sigma}} \mathrm{d}A\mathrm{d}\bar{z} - \delta \hat{\mathbf{d}}^{\mathrm{T}} \hat{\mathbf{f}} = 0 \tag{15}$$

where $\hat{\boldsymbol{\varepsilon}}$ represents the vector of strain components of the shell element. The potential energy functional is modified according to [31] to prevent numerical stability issues with the Allman type interpolations of the membrane displacements. The stress vector is obtained by assuming linear elastic material.

3.1 Constitutive relations for the shell element

For a laminate composed of n orthotropic layers, the orientation of the fibre-attached $x_k y_k$-axes with respect to the plate's local xy axes is determined by the angle Φ which is the angle about plate's local z-axis (positive according to the right hand rule) between x and x_k (Figure 3(a)). In that case, Φ is the same angle used section 2.1.

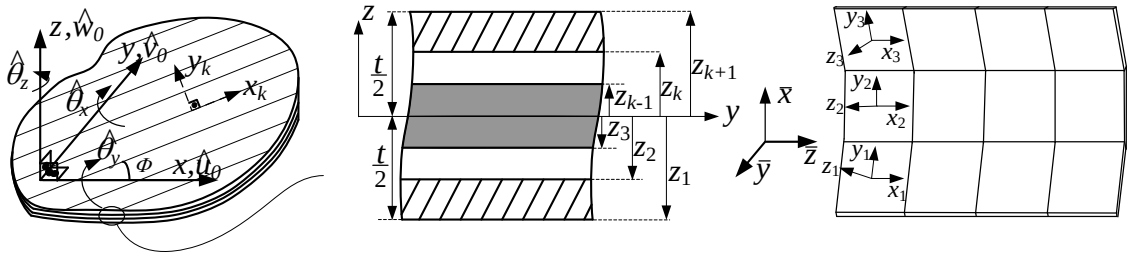

(a) Shell local coordinates (b) Laminates across thickness (c) Global vs. local coordinates

Figure 3: Deflections and coordinate system of the shell composed of fiber-reinforced laminates

Assuming that perfect interlaminar bond exists between the layers, the stress-strain relationship for the k^{th} layer according to the plate local axis directions can be written as [29]

$$\hat{\boldsymbol{\sigma}}^{(k)} = \begin{Bmatrix} \hat{\sigma}_x^{(k)} \\ \hat{\sigma}_y^{(k)} \\ \hat{\tau}_{xy}^{(k)} \\ \hat{\tau}_m^{(k)} \end{Bmatrix} = \hat{\mathbf{Q}}^{(k)} \hat{\boldsymbol{\varepsilon}} \tag{16}$$

where

$$\hat{\mathbf{Q}}^{(k)} = \begin{bmatrix} \bar{Q}_{11}^{(k)} & \bar{Q}_{12}^{(k)} & \bar{Q}_{16}^{(k)} & 0 \\ \bar{Q}_{12}^{(k)} & \bar{Q}_{22}^{(k)} & \bar{Q}_{26}^{(k)} & 0 \\ \bar{Q}_{16}^{(k)} & \bar{Q}_{26}^{(k)} & \bar{Q}_{66}^{(k)} & 0 \\ 0 & 0 & 0 & \bar{Q}_{66}^{(k)} \end{bmatrix} \tag{17}$$

in which the coefficients are as given in [9-11,35]. It should be noted that the last diagonal term in Equation (17) is because of the modification introduced into the potential energy functional (also see [29]).

4 MULTI-SCALE ANALYSIS

Fig. 4 shows a schematic of the multi-scale analysis performed. The total domain is shown by Ω_m in the figure, which is modelled by a beam-type finite element. The critical part of the beam – depicted by Ω_c in the figure – is a subset of Ω_m and is modelled by shell elements.

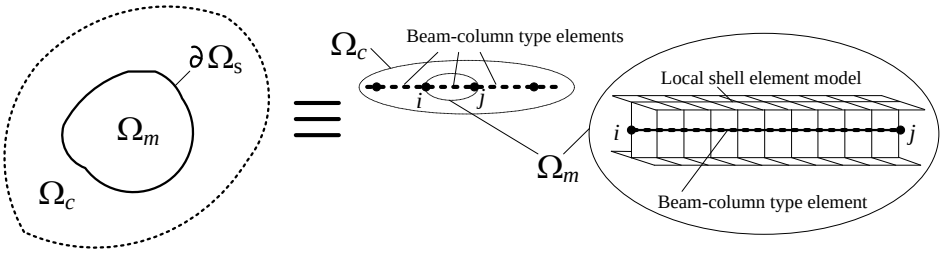

Figure 4: Decomposition of the analysis domain

Based on the bridging multiscale method (BMM) the shell nodal displacement vector is decomposed into a coarse-scale component and a difference term. To this end, a decomposition matrix *N* is used, which projects the beam results onto the nodal points of the shell model, i.e. $\hat{\mathbf{d}} = \mathbf{X}\bar{\mathbf{d}} + \mathbf{d}'$, from which the variation of the shell nodal displacement vector can be written as

$$\delta\hat{\mathbf{d}} = \mathbf{N}\delta\bar{\mathbf{d}} + \delta\mathbf{d}' \tag{18}$$

in which the relation $\mathbf{N}\delta\bar{\mathbf{d}} = \mathbf{X}\delta\bar{\mathbf{d}} + \delta\mathbf{X}\bar{\mathbf{d}}$ was used. As a result, the strain vector of the shell model can be decomposed into two parts: $\hat{\boldsymbol{\varepsilon}} = \bar{\boldsymbol{\varepsilon}} + \boldsymbol{\varepsilon}'$, in which the term $\bar{\boldsymbol{\varepsilon}}$ refers to the strain due to the beam formulation. Consequently, the stress vector can be decomposed in the

same fashion as $\hat{\boldsymbol{\sigma}} = \bar{\boldsymbol{\sigma}} + \boldsymbol{\sigma}'$. By introducing these values into the variational form of the shell element i.e. Eq. (10), the equilibrium requires the simultaneous satisfaction of the two equations as

$$\delta\Pi_1 = \delta\bar{\mathbf{d}}^{\mathrm{T}}\mathbf{N}^{\mathrm{T}}\int_L\int_A \hat{\mathbf{B}}^{\mathrm{T}}\hat{\mathbf{S}}^{\mathrm{T}}\bar{\boldsymbol{\sigma}}\mathrm{d}A\mathrm{d}\bar{z} - \delta\bar{\mathbf{d}}^{\mathrm{T}}\mathbf{N}^{\mathrm{T}}\hat{\mathbf{f}} + \delta\bar{\mathbf{d}}^{\mathrm{T}}\mathbf{F} = 0 \tag{19}$$

$$\delta\Pi_2 = \delta\mathbf{d}'^{\mathrm{T}}\int_L\int_A \hat{\mathbf{B}}^{\mathrm{T}}\hat{\mathbf{S}}^{\mathrm{T}}\hat{\boldsymbol{\sigma}}\mathrm{d}A\mathrm{d}\bar{z} - \delta\mathbf{d}'^{\mathrm{T}}\,\mathbf{f} = 0 \tag{20}$$

The two later equations are linearized to form the basis for the finite element formulation. The shell solution is obtained by imposing the displacement filed of the beam element as an interface boundary condition for the shell element. Therefore, the procedure is as follows: firstly, the global problem (i.e. the beam model) is solved to result in the displacement filed $\bar{\mathbf{d}}$ while keeping the fine-scale solution of the local shell model fixed. Then the local model (i.e. the local shell) is solved by the imposition of the global displacement as interface boundary conditions to find values of $\hat{\mathbf{d}}$. Two criteria are checked to ensure the convergence in each load step as suggested by [32] within the framework of BMM. The first criterion is due to geometric nonlinearity, which confirms that the global equilibrium is achieved at the end of n iterations. Secondly, the difference in the stress vectors of the local shell and the beam model should vanish to ensure that the two solutions are synchronized. In each iteration, the difference between the stress vectors are applied to the model as a complementary force until this force is smaller than a predefined tolerance.

5 APPLICATIONS

Based on the procedure discussed in previous sections, two numerical experiments are performed to ensure the applicability of the method. In all cases, the results from the multi-scale procedure are compared with those of the full shell-type model for verification purposes. In order to ensure that the beam-type analysis is kinematically equivalent to the shell model, the comparison with the constraint shell solution is also presented. The constraint shell model is obtained by applying multiple-point constraints (MPCs) on the nodal displacement of the shell model based on the decomposition matrix N, discussed in section 4. For both examples considered herein the material is taken as glass-epoxy for which the material properties are provided in table 1.

Table 1: Values of material properties for glass-epoxy composite

E_1	E_2	G_{12}	G_{13}	G_{23}	υ_{12}	υ_{21}
53.78 GPa	17.93 GPa	8.96 GPa	8.96 GPa	3.45 GPa	0.25	0.08

5.1 Flexural buckling of a C- section column

The developed method is used for the buckling analysis of a composite column as illustrated in Fig. 5

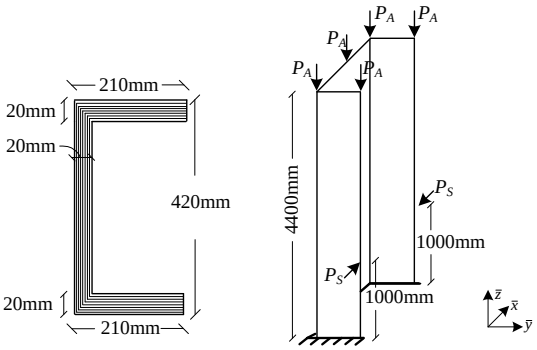

Figure 5: Dimensions, loading and the boundary conditions of the C-section column

The analysis was performed for equal thickness angle-ply lay-ups of $[0/-45/90/45]_{2S}$. Four equal-span beam-type elements were used for the analyses, and the shell element dimensions were $200\,mm \times 200\,mm$ in all cases. Firstly, the load versus tip deflection and rotation relationships were obtained only under tip loading, so as not to cause local deformation (i.e. $P_A = 50kN$, and $P_S = 0$ as shown in Fig. 5). The buckling loads based on the linearized buckling analysis corresponding to beam-type, constraint-shell-type and full-shell-type analysis are $P_{Acr} = 52.19kN$, $P_{Acr} = 52.12kN$ and $P_{Acr} = 53.48kN$, respectively. The Euler buckling load can be calculated from $N_{cr} = \pi^2 EI/(2L)^2$, where L is the column length and is the flexural rigidity of the composite cross-section about the minor principal axis, and it is $N_{cr} = 259.66kN$, based on which can be obtained as $P_{Acr} = 51.93kN$.

In Figure 6, the results produced from the linear static and nonlinear analyses are shown based on full beam and shell-type and constraint shell-type models. All solutions agree well for $P_A = 50kN$, and $P_S = 0$. Additionally to $P_A = 50kN$,, when a load $P_S = 75kN$ is applied to cause local deformations, the results based on beam- and constraint shell-type analysis are not affected but those based on the full shell-type are significantly affected, as shown in Figure 6. For the multi-scale analysis, the overlapping region was first considered between $\bar{z} = 0$ and $\bar{z} = 1200mm$ by using 6×4 elements and then considered between $\bar{z} = 0$ and $\bar{z} = 1600mm$ by using 8×4 elements.

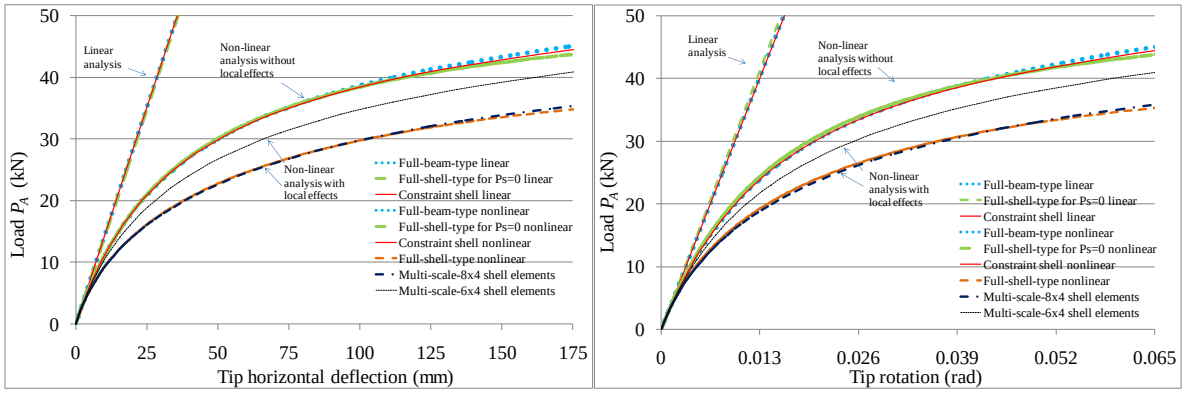

(a) Tip horizontal deflection (b) Tip rotation

Figure 6: Load-deflection relations based on different modelling types

5.2 Flexural buckling analysis of a simply supported I-beam

In the second case, a simply-supported beam subjected to a moment gradient is analysed. The dimensions of the beam and its support conditions are given in Figure 7.

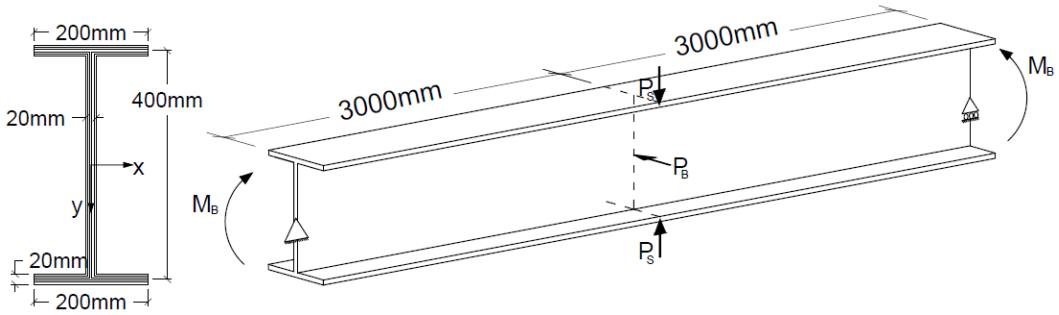

Figure 7: Dimensions, loading and the boundary conditions of the I-section beam

Eight equal-span beam-type elements were used for the analyses and the shell element dimensions were $200\ mm \times 200\ mm$ in all cases. The flanges and the web were laminated symmetrically, and angle-ply lay-ups of $[0/-45/90/45/45/90/-45/0]_{2S}$ were used. The moment versus mid-span horizontal and vertical deflections obtained under the loading scheme are shown in Figure 7(b).

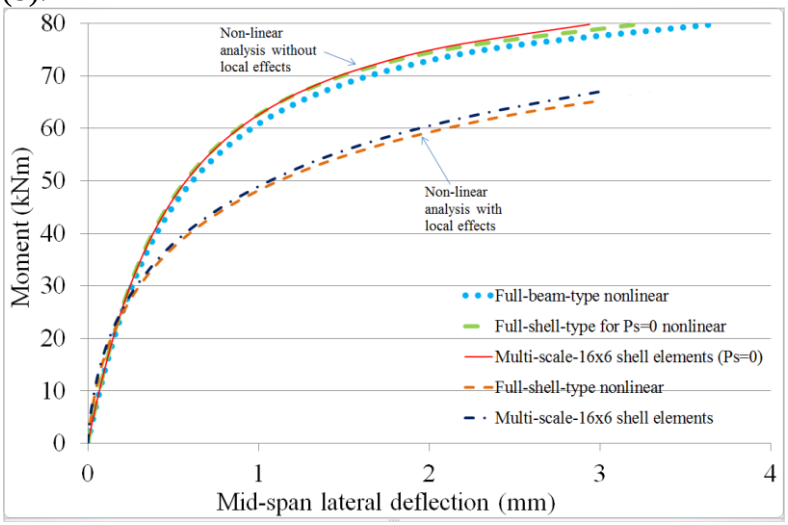

Figure 8: Load-deflection relations based on different modelling types

In this figure, the results of the nonlinear analyses are shown based on full beam- and shell-type and multi-scale models under $M_B = 80kNm$, $P_B = 0.1kN$. It can be verified that when $P_S = 0$, the results based on full beam- and shell-type and multi-scale are in very good agreement. In order to stimulate local deformations, a force couple of $P_S = 15kN$ was added at the tips of right top and bottom flanges in opposite directions as shown in Fig. 7. In this case, the horizontal deflections at the mid-span increase significantly as can be seen from the results of the full shell-type analysis in Figure 8. In that case, the beam solution is not capable of capturing the behaviour due to rigid cross-section assumption. However, it can be verified

that multi-scale analysis results agree very well with the shell solution under local effects. For multi-scale analysis, the overlapping region is considered between $\bar{z} = 1400mm$ and $\bar{z} = 4600mm$ by using 16×6 elements.

6 CONCLUSIONS

In this paper, a multiscale analysis method based on the BMM was developed for the analysis of composite thin-walled members to incorporate the effects of local deformations on the global behaviour of the thin-walled member by using a shell model only within the region of local deformations. It was illustrated through examples that by selecting sufficiently wide span of the local shell model, the proposed multiscale analysis is capable to capture the behaviour accurately.

REFERENCES

[1] Bauld NR, Tzeng LS. A Vlasov theory for fiber-reinforced beams with thin-walled open cross-sections. *International Journal of Solids and Structures* 1984; **20**: 277-297.

[2] Pandey MD, Kabir MZ, Sherbourne AN. Flexural-torsional stability of thin-walled composite I-section beams. *Composites Engineering* 1995; **5**(3):321–342.

[3] Kollar LP. Mechanics of laminated composite plates and shells. *International Journal of Solids and Structures* 1991; **38**:7525-7541.

[4] Sapkas A, Kollar LP. Lateral torsional buckling of composite beams. *International Journal of Solids and Structures* 2002; **39**:2939-2963.

[5] Kim N-I, Shin DK, Kim M-Y. Exact lateral buckling analysis for thin-walled composite beams under end moment. *Engineering Structures* 2007; **29**:1739-1751.

[6] Omidvar B, Ghorbanpoor A. Nonlinear FE solution for thin-walled open section composite beams. *Journal of Structural Engineering, ASCE* 1996; **122**: 1369-1378.

[7] Lee J, Kim S-E, Hong K. Lateral buckling of I-section composite beams. *Engineering Structures* 2002; **24**:955-964.

[8] Lee J. Lateral buckling analysis of thin-walled laminated composite beams with monosymmetric sections. *Engineering Structures* 2006; **28**:1997-2009.

[9] Back SY, Will KM, Hong K. Shear flexible thin-walled element for composite I- beams. *Engineering Structures* 2008; **30**:1447-1458.

[10] Cardoso JEB, Benedito NMB, Valido AJJ. Finite element analysis of thin-walled composite beams with geometrically nonlinear behaviour including warping deformation. *Thin-Walled Structures* 2009; **47**:1363-1372.

[11] Belytschko T, Korungauz Y, Organ D, Fleming M, Krysl P. Meshless methods: An overview and recent developments. *Computer Methods in Applied Mechanics and Engineering* 1996; **139**:3-47.

[12] Erkmen RE, Bradford MA. Coupling of finite element and meshfree methods for locking-free analysis of shear deformable beams and plates. *Engineering Computations* 2011; **28**: 1003-1027.

[13] Babuska I, Melenk JM. The partition of unity finite element method. *International Journal for Numerical Methods in Engineering* 1997; **40**:727-758.

[14] Belytschko T, Moes N, Usui S, Parimi C. Arbitrary discontinuities in finite elements. *International Journal for Numerical Methods in Engineering* 2001; **50**:993-1013.

[15] Fish J, Markolefas S, Guttal R, Nayak P. On adaptive multilevel superposition of finite element meshes for linear elastostatics. *Applied Numerical Mathematics* 1994; **14**:135-164.
[16] Hughes TJR, Fiejoo G, Mazzei L, Quincy JB. The variational multiscale method- a paradigm for computational mechanics. *Computer Methods in Applied Mechanics and Engineering* 1998; **166**:3-24.
[17] Hughes TJR, Sangalli G. Variational multiscale analysis: The fine-scale Green's function, projection, optimization, localization and stabilized methods. *SIAM Journal of Numerical Analysis* 2007; 45: 539-557.
[18] Liu WK, Hao S, Belytschko T, Li S, Chang CT. Multi-scale methods. *International Journal for Numerical Methods in Engineering* 2000; **50**:993-1013.
[19] Feyel F. A multi-level finite element method to describe the response of highly nonlinear structures using generalized continua. *Computer Methods in Applied Mechanics and Engineering* 2003; **192**:3233-3244.
[20] Geers MGD, Kouznetsova VG, Brekelmans WAM. Multi-scale computational homogenization: Trends and challenges. *Journal of Computational and Applied Mathematics* 2010; **234**:2175-2182.
[21] Liu WK, Uras RA, Chen Y. Enrichment of the finite element method with the reproducing kernel particle method. *Journal of Applied Mechanics, ASME* 1997; **64**(4):861-870.
[22] Kadowaki H, Liu WK. Bridging multi-scale method for localization problems. *Computer Methods in Applied Mechanics and Engineering* 2004; **193**:3267-3302.
[23] Bradford, MA, Hancock GJ. Elastic interaction of local and lateral buckling in beams. *Thin-walled Structures* 1984; **2**:1-25.
[24] Bradford MA (1992). Lateral-distortional buckling of steel I-section members. *Journal of the Constructional Steel Research* 1992; **23**:97-116.
[25] Davies JM and Leach P. Second-order generalized beam theory. *Journal of the Constructional Steel Research* 1994; **31**:221-241.
[26] Ronagh HR, Bradford MA. A rational model for distortional buckling of tapered members. *Computer Methods in Applied Mechanics and Engineering* 1996; **130**:263-277.
[27] Erkmen RE. Bridging multi-scale approach to consider the effects of local deformations in the analysis of thin-walled members. *Computational Mechanics* 2013; 52 (1), pp. 65-79.
[28] Trahair NS. *Flexural-Torsional Buckling of Structures*. London: Spon Press, 2003.
[29] Reddy JN. *Mechanics of Laminated Composite Plates and Shells: Theory and Analysis.* 2nd edn. Boca Raton, Florida: CRC Press.
[30] Batoz J-L, Tahar MB. Evaluation of a new quadrilateral thin plate bending element. *International Journal for Numerical Methods in Engineering* 1982; **18**:1655-1677.
[31] Ibrahimbegovic A, Taylor RL, Wilson EL. A robust quadrilateral membrane finite element with drilling degrees of freedom. *International Journal for Numerical Methods in Engineering* 1990; **30**:445-457.
[32] Qian D, Wagner GJ, Liu WK. A Multi-scale projection method for the analysis of carbon nanotubes. Comput Methods Appl Mech Eng 2004; 193: 1603–1632